A First Glance into Mixed Phosphine-Stibine Moieties as Protecting Ligands for Gold Clusters

Kundan K. Singh[#1], Ayan Bhattacharyya[#1], Shana Havenridge[2], Mohamed Ghabin[1], Hagan Ausmann[1], Maxime A. Siegler[3], Christine M. Aikens*[2] and Anindita Das*[1]

1: Department of Chemistry, Southern Methodist University, Dallas, Texas 75275, United States.
2: Department of Chemistry, Kansas State University, Manhattan, Kansas 66506, United States.
3: Department of Chemistry, Johns Hopkins University, Baltimore, Maryland 21218, United States.

#: K.K.S and A.B. contributed equally to this work.
Emails: cmaikens@ksu.edu (theory); aninditad@smu.edu (experiment)

Table of Contents (TOC)

Fig. S10: Molecular orbitals at the BP86-D3/DZP level of theory for the H-3→L+7 and H-3→L+5 transitions in the 3.30 eV peak.

Fig. S11: Molecular orbitals at the BP86-D3/DZP//BP86-D3/DZP (left) and LRCF-D3/DZP//BP86-D3/DZP (right) levels of theory along with the corresponding orbital energy.

Fig. S12: Molecular orbitals at the BP86-D3/DZP//BP86-D3/DZP (left) and LRCF-D3/DZP//BP86-D3/DZP (right) levels of theory along with the corresponding orbital energy for LUMO+1 – HOMO-1.

Fig. S13: Molecular orbitals at the BP86-D3/DZP//BP86-D3/DZP (left) and LRCF-D3/DZP//BP86-D3/DZP (right) levels of theory along with the corresponding orbital energy for HOMO-2 – HOMO-5.

Fig. S14: Absorption spectrum of $[Au_6(SbP_3)_2]^{2+}$ at (A) BP86-D3/DZP//BP86-D3/DZP level of theory and (C) LRCF-D3/DZP//BP86-D3/DZP level of theory. Absorption spectrum of $[Au_6(PPh_3)_6]^{2+}$ at (B) BP86-D3/DZP//BP86-D3/DZP level of theory and (D) LRCF-D3/DZP//BP86-D3/DZP level of theory. (FWHM = 0.20 eV)

Fig. S15: Molecular orbital details at the LRCF-D3/DZP level of theory at the BP86-D3/DZP S_0 geometry for $[Au_6(PPh_3)_6]^{2+}$. (A) Atomic orbital contributions to molecular orbitals and (B) Molecular orbitals responsible for the 3.44 eV peak.

Fig. S16: Molecular orbitals at the LRCF-D3/DZP level of theory on the BP86-D3/DZP S_0 geometry for (A) the H→L+2 transition in the 3.14 eV peak in $[Au_6(SbP_3)_2]^{2+}$ and (B) the H→L+2 transition in the 3.44 eV peak in $[Au_6(PPh_3)_6]^{2+}$.

Fig. S17: Molecular orbitals at the LRCF-D3/DZP level of theory on the BP86-D3/DZP S_0 geometry for (A) the H→L transition in the 2.93 eV peak in $[Au_6(SbP_3)_2]^{2+}$ and (B) the H→L+1 transition in the 2.88 eV peak in $[Au_6(PPh_3)_6]^{2+}$.

Fig. S18: Time-dependent UV–visible spectral study of thermal stability of a toluene solution of the $[Au_6(SbP_3)_2][PF_6]_2$ cluster at 70 °C.

S1.4 Structure and Synthesis of SbP_2.

Fig. S19: The ^{1}H-NMR spectra of SbP_2.

Fig. S20: ^{31}P-NMR spectra of SbP_2.

Fig. S21: Time-dependent UV–vis spectra of the cluster formation reaction with SbP_2 ligand.

Fig. S22: Picture of the insoluble black precipitate which the unstable Au clusters formed with SbP_2 ligand convert to over time.

Fig. S23: Crystal packing in the unit cell of the $[Au_6(PPh_3)_2][PF_6]_2$ structure.

S1.1 Synthesis of the ligand SbP_3.

The synthesis of the ligand is based on reported procedures with minor modifications.[1-2] 500 mg (1.465 m-moles) of (2-bromophenyl) diphenyl phosphine is dissolved in dry diethylether in a 2-necked round-bottomed (RB) flask, inside the glove-box. The RB-flask is tightly sealed, put under N_2-balloon and cooled to -78°C in acetonitrile-dry ice bath. Then, 1 mL (1.6 M) n-butyllithium is slowly added using a syringe. The reaction mixture is allowed to stir for 30 minutes at -78°C. Then, 110 mg (0.482 m-moles) of antimony-trichloride ($SbCl_3$) dissolved in dry diethylether (inside glove box) is slowly added using a syringe, while maintaining the temperature at -78 °C. Beyond this addition, the reaction mixture is allowed to warm up to room temperature and kept under stirring condition overnight. The product forms as a white precipitate which is then filtered, washed several times with diethylether, dried and characterized using NMR.

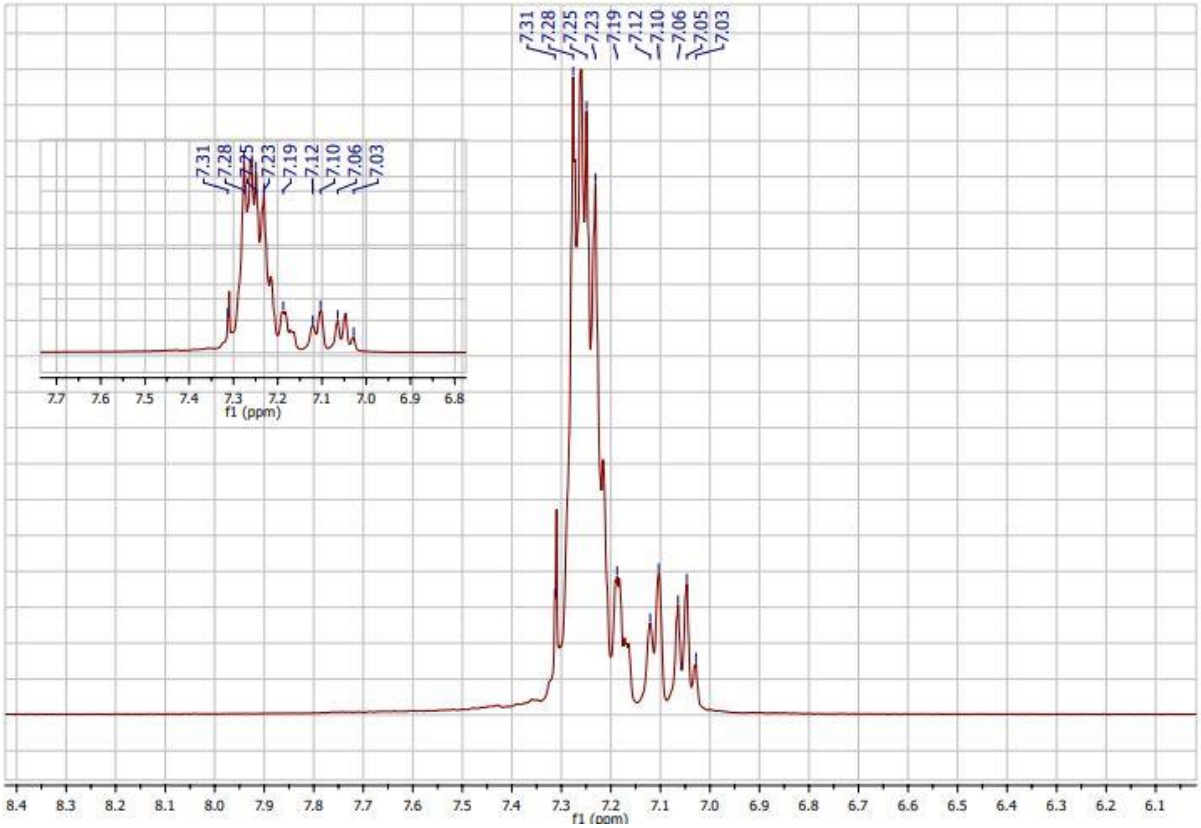

Fig. S1 The ^{1}H-NMR spectra of SbP_3 in $CDCl_3$ showing peaks at d (ppm) = 7.03 (singlet), 7.05-7.06 (doublet), 7.10-7.12 (doublet), 7.19 (singlet), 7.31-7.23 (multiplet, merged with $CDCl_3$ peak).

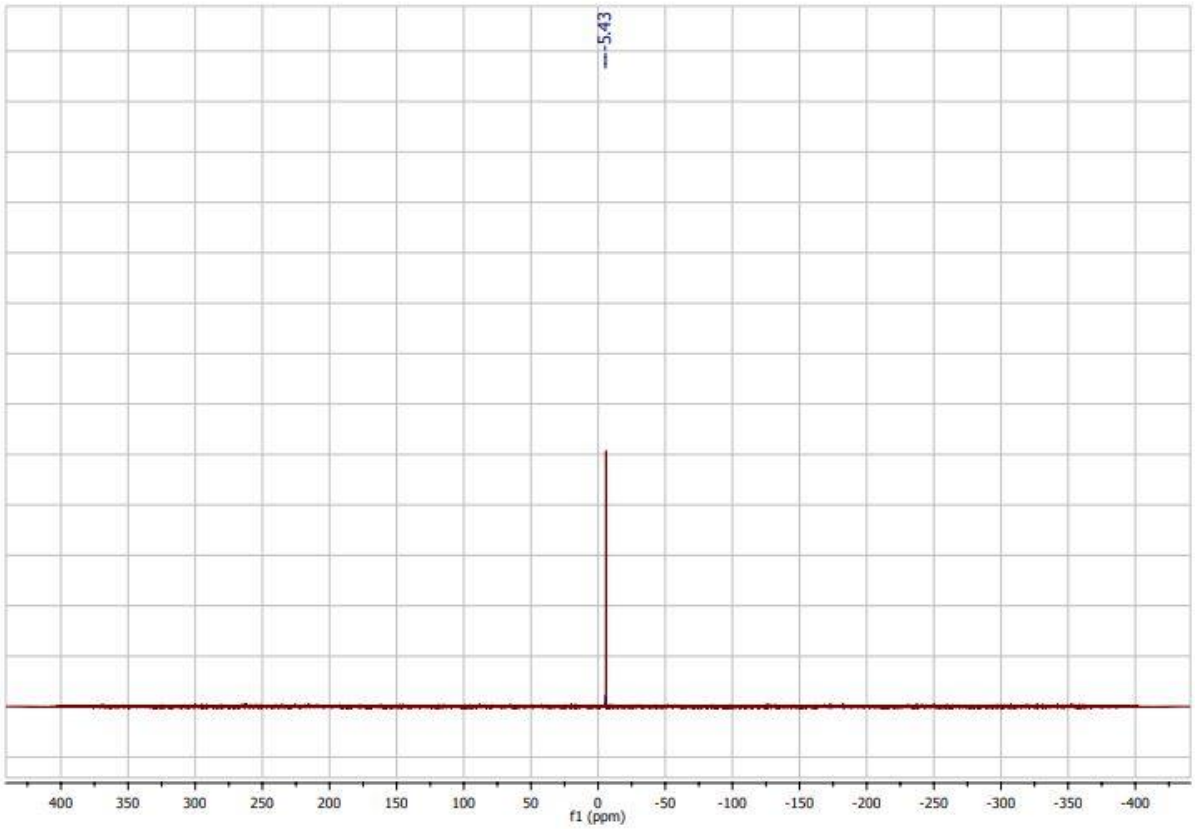

Fig. S2 The ^{31}P-NMR spectra of SbP_3 in $CDCl_3$ showing only one characteristic peak at d (ppm) = -5.43.

S1.2 Detailed synthesis of $[Au_6(SbP_3)_2][PF_6]_2$

5 mg (0.0169 m-moles) of chloro-dimethylsulphide Au-(I) is dissolved in 1 mL DCM in vial-1 and 14 mg (0.0154 m-moles) SbP_3 is dissolved in 1 mL DCM in vial-2. The complete solubility for each vial is ensured via sonication. Then, the contents of vial-2 are slowly added to vial-1 in a dropwise manner. The mixture is allowed to stir for 30 minutes. Then, 1.2 mg (0.317 mmoles) $NaBH_4$ dissolved in 0.5 mL ethanol is slowly added to the reaction mixture in a dropwise manner. The reaction is allowed to run for 2 hours. Then, the volume of the reaction mixture is reduced to 1 mL via purging N_2 gas. The 1 mL solution is divided into two centrifuge tubes (0.5 mL each) and 5 mL diethyl ether is added to each of the tubes and centrifuged for 6 minutes at 4000 rpm. The brown-red solid obtained as precipitate is dissolved in 3 mL ethanol and to it an excess (c.a. 200 mg) of $NaPF_6$ is added. The mixture is stirred for 2 hours, and the orange-red precipitate is collected via centrifugation. Then the precipitate is dissolved in 1 mL DCM, sonicated, and then centrifuged to remove insoluble side-products. Finally, single crystals are grown by diffusing pentane into the DCM solution at 4°C (yield ~35% Au atom basis).

S1.3 Experimental Details of Single-Crystal X-Ray Measurements

All reflection intensities were measured at 110(2) K using a SuperNova diffractometer (equipped with Atlas detector) with Mo *K*α radiation (λ = 0.71073 Å) under the program CrysAlisPro (Version CrysAlisPro 1.171.39.29c, Rigaku OD, 2017). The same program was used to refine the cell dimensions and for data reduction. The structure was solved with the program SHELXS-2018/3 (Sheldrick, 2018) and

was refined on F^2 with SHELXL-2018/3 (Sheldrick, 2018). Analytical numeric absorption correction using a multifaceted crystal model was applied using CrysAlisPro. The temperature of the data collection was controlled using the system Cryojet (manufactured by Oxford Instruments). The H atoms were placed at calculated positions using the instructions AFIX 23 or AFIX 43 with isotropic displacement parameters having values 1.2 U_{eq} of the attached C atoms.

The asymmetric unit contains two crystallographically independent halves of Au_6 clusters (the two Au_6 clusters are found at sites of inversion symmetry), two PF_6^- counterions and some amount of lattice DCM solvent molecules (two partially occupied DCM molecules were treated as ordered, and the values of the occupancy factors refine to 0.939(8) and 0.892(8)). The structure is partly disordered as six phenyl groups and the two PF_6^- counterions are disordered over two orientations. All occupancy factors of the major components of the disorder can be retrieved from the final .cif file. The asymmetric unit also contains some amount of partially occupied and disordered lattice DCM solvent molecules, and their contribution was removed from the final refinement using the SQUEEZE procedure in Platon (Spek, 2009).

Table S1 Crystallographic data for $[Au_6(SbP_3)_2][PF_6]_2$

	$[Au_6(SbP_3)_2][PF_6]_2$
Crystal data	
Chemical formula	$C_{108}H_{84}Au_6P_6Sb_2{\cdot}2(F_6P){\cdot}1.831(CH_2Cl_2)$
M_r	3438.16
Crystal system, space group	Triclinic, *P*-1
Temperature (K)	110
a, *b*, *c* (Å)	14.2806 (3), 18.2744 (6), 22.8464 (6)
α, β, γ (°)	80.353 (3), 75.399 (2), 80.671 (2)
V (Å^3)	5643.0 (3)
Z	2
Radiation type	Mo *K*α
μ (mm^{-1})	8.50
Crystal size (mm)	0.21 × 0.12 × 0.03
Data collection	
Diffractometer	SuperNova, Dual, Cu at zero, Atlas
Absorption correction	Analytical *CrysAlis PRO* 1.171.41.93a (Rigaku Oxford Diffraction, 2020) Analytical numeric absorption correction using a multifaceted crystal model based on expressions derived by R.C. Clark & J.S. Reid. (Clark, R. C. & Reid, J. S. (1995). Acta Cryst. A51, 887-897) Empirical absorption correction using spherical harmonics, implemented in SCALE3 ABSPACK scaling algorithm.
T_{min}, T_{max}	0.281, 0.805

No. of measured, independent and observed [$I > 2\sigma(I)$] reflections	74920, 19846, 15987
R_{int}	0.048
$(\sin \theta/\lambda)_{max}$ (Å^{-1})	0.595
Refinement	
$R[F^2 > 2\sigma(F^2)]$, $wR(F^2)$, S	0.038, 0.100, 1.02
No. of reflections	19846
No. of parameters	1721
No. of restraints	1689
H-atom treatment	H-atom parameters constrained
	$w = 1/[\sigma^2(F_o^2) + (0.0513P)^2 + 24.8589P]$ where $P = (F_o^2 + 2F_c^2)/3$
$\Delta\rho_{max}$, $\Delta\rho_{min}$ (e Å^{-3})	2.57, -1.61

Computer programs: *CrysAlis PRO* 1.171.39.29c (Rigaku OD, 2017), *SHELXS2018*/3 (Sheldrick, 2018), *SHELXL2018*/3 (Sheldrick, 2018), *SHELXTL* v6.10 (Sheldrick, 2008).

References:

Sheldrick, G. M. (2015). Acta Cryst. C71, 3-8.
Spek, A.L. (2009). Acta Cryst. D65, 148-155.

Summary of bond-lengths for one of the two crystallographically independent $Au_6(SbP_3)_2]^{2+}$ cations obtained from single crystal X-ray crystallography.

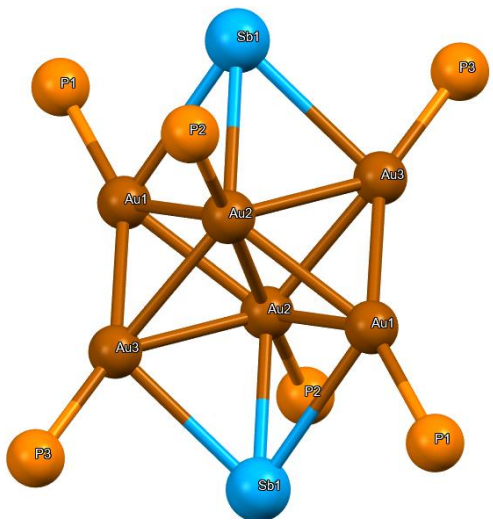

Table S2 Selected bond distances for $Au_6(SbP_3)_2]^{2+}$ (Å)

Au1	Au3	2.7160(4)
Au1	Au2	2.7764(4)
Au1	Au2	2.7898(4)
Au1	Sb1	3.1906(6)
Au2	P2	2.2978(19)
Au2	Au2	2.6682(5)
Au2	Au3	2.7485(4)
Au2	Au3	2.8245(4)
Au2	Sb1	3.0079(6)
Au3	P3	2.295(2)
Au3	Sb1	3.0479(6)
Au1	P1	2.296(2)

Table S3 Average bond distances of the two $[Au_6(SbP_3)_2]^{2+}$ monomers and $[Au_6(PPh_3)_6]^{2+}$ in the crystal structure[3] and optimized ground state geometry at the BP86-D3/DZP level of theory.

Average Bond Distance (Å)	Au-Au Bonds	Au-Sb Bonds	Au-P Bonds	Sb-C Bonds	P-C Bonds
$[Au_6(SbP_3)_2]^{2+}$ Crystal	**2.760**	**3.095**	**2.293**	**2.173**	**1.823**
	0.048	0.137	0.004	0.018	0.011
BP86-D3/DZP S_0	**2.781**	**3.078**	**2.302**	**2.202**	**1.819**
	0.064	0.018	0.011	0.008	0.007
$Au_6(PPh_3)_6$ Crystal[3]	**2.713**		**2.352**		**1.818**
	0.141		0.119		0.004
$Au_6(PPh_3)_6$ BP86-D3/DZP S_0	**2.774**		**2.307**		**1.818**
	0.045		0.009		0.004

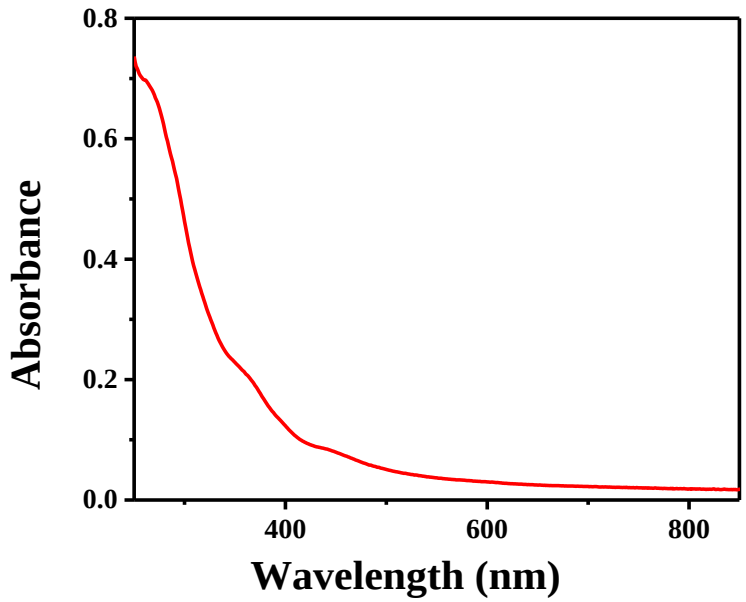

Fig. S3 UV-vis absorption spectra of $[Au_6(SbP_3)_2][PF_6]_2$ in ethanol displaying two characteristic bands centered around 368 nm and 462 nm, respectively.

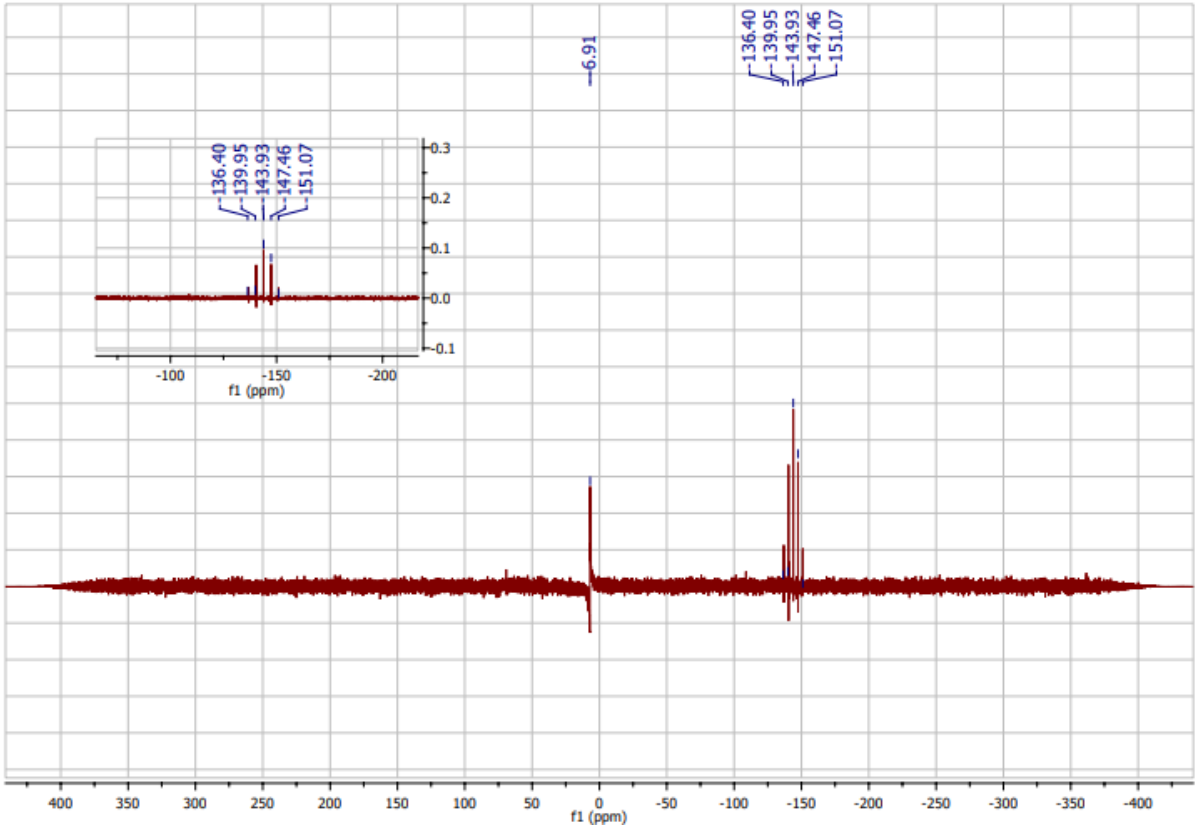

Fig. S4 The ^{31}P NMR data of $[Au_6(SbP_3)_2][PF_6]_2$ displaying a peak at d = 6.91 ppm for the cluster and 5 peaks lying between -136 ppm to -152 ppm, which are from the PF_6- counter-ion.

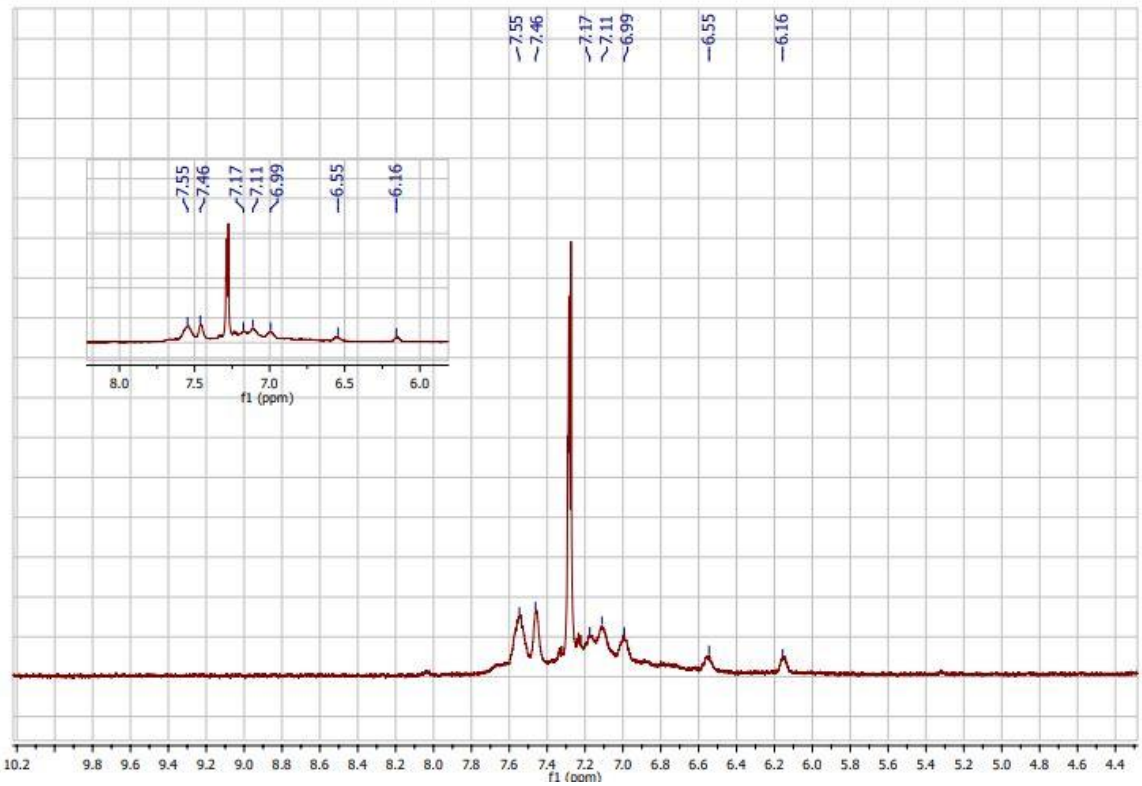

Fig. S5 The ^{1}H NMR data of $[Au_6(SbP_3)_2][PF_6]_2$ displaying peaks at d = 6.16, 6.55, 6.99, 7.11,7.17,7.46 and 7.55 ppm.

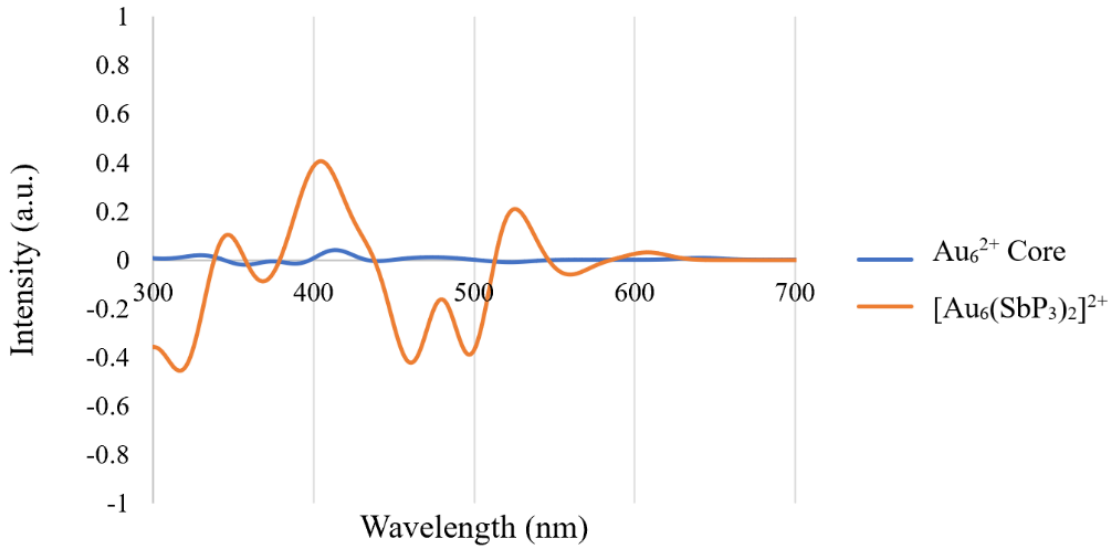

Fig. S6 Theoretical circular dichroism spectrum at the BP86-D3/DZP level of theory.

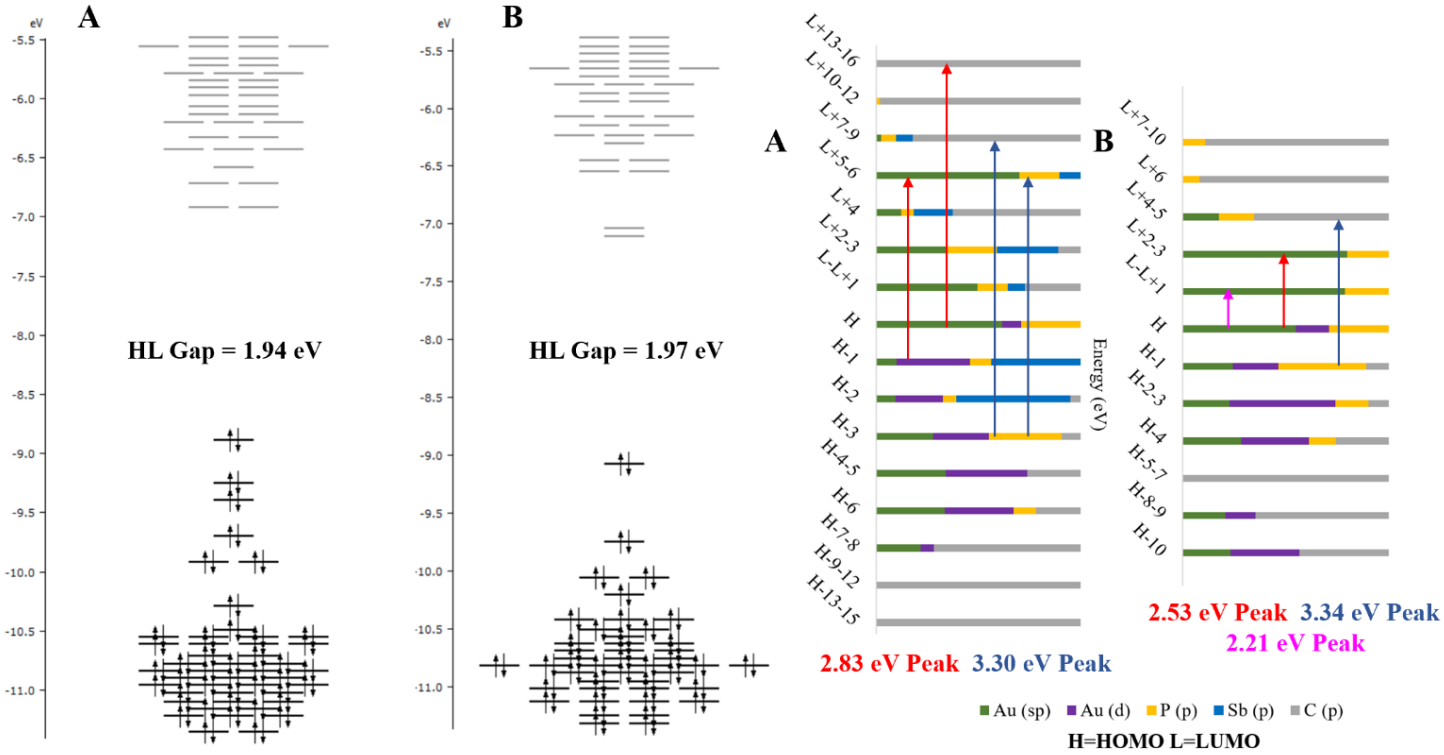

Fig. S7 Molecular orbital details at the BP86-D3/DZP level of theory. Molecular orbital diagram (left) and atomic orbital contributions to molecular orbitals (right) of (A) $[Au_6(SbP_3)_2]^{2+}$ and (B) $[Au_6(PPh_3)_6]^{2+}$.

Table S4 Comparison of vertical energies between BP86-D3/DZP//BP86-D3/DZP and LRCF-D3/DZP//BP86-D3/DZP of the peaks displayed in the theoretical absorption spectra.

Peak	BP86-D3/DZP//BP86-D3/DZP	LRCF-D3/DZP//BP86-D3/DZP
(a)	2.34	2.93
(b)	2.83	3.14
(c)	3.06	3.62
(d)	3.30	3.89
(e)	3.67	4.16

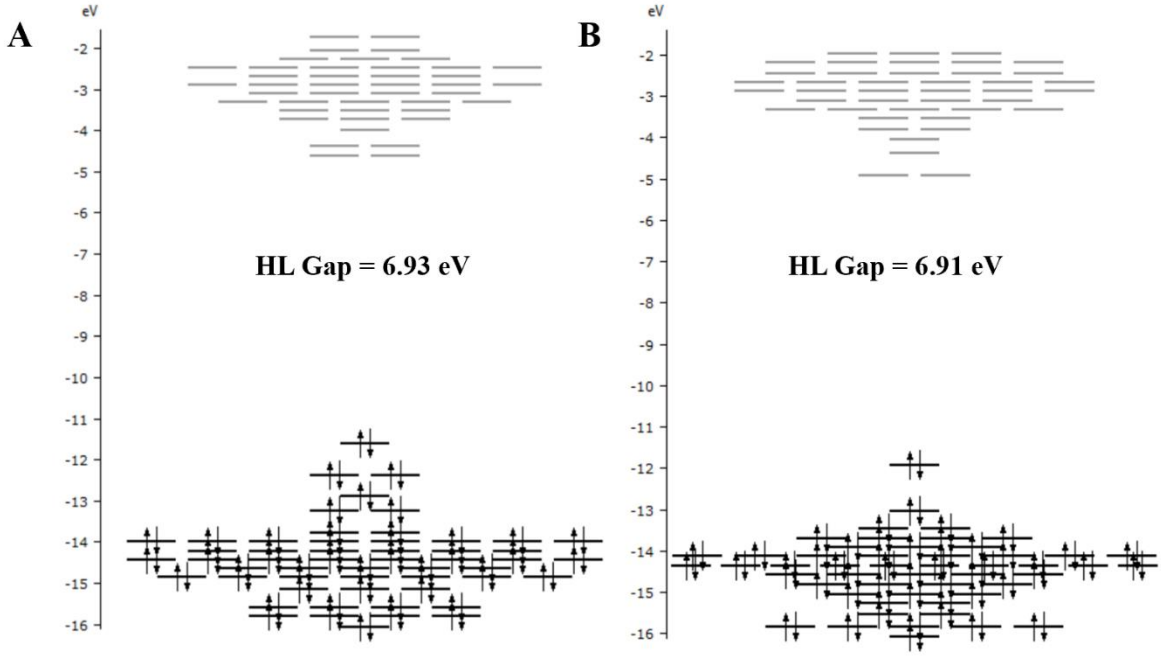

Fig. S8 Molecular orbital details at the LRCF-D3/DZP level of theory at the BP86-D3/DZP S_0 geometry. Molecular orbital diagram of (A) $[Au_6(SbP_3)_2]^{2+}$ and (B) $[Au_6(PPh_3)_6]^{2+}$.

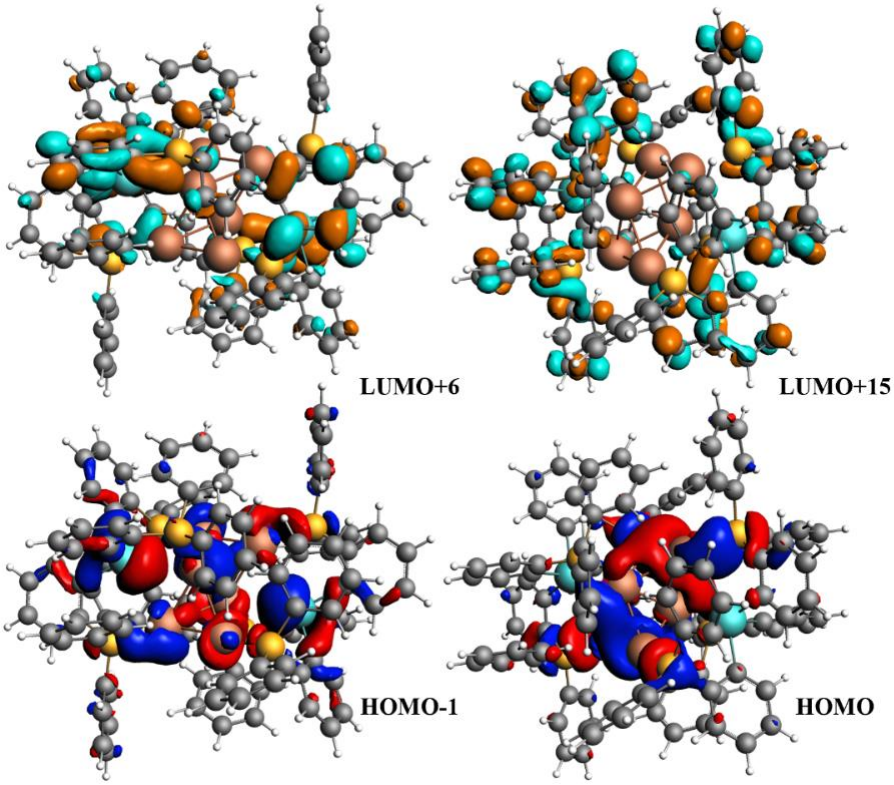

Fig. S9 Molecular orbitals at the BP86-D3/DZP level of theory for the H-1→L+6 and H→L+15 transitions in the 2.83 eV peak.

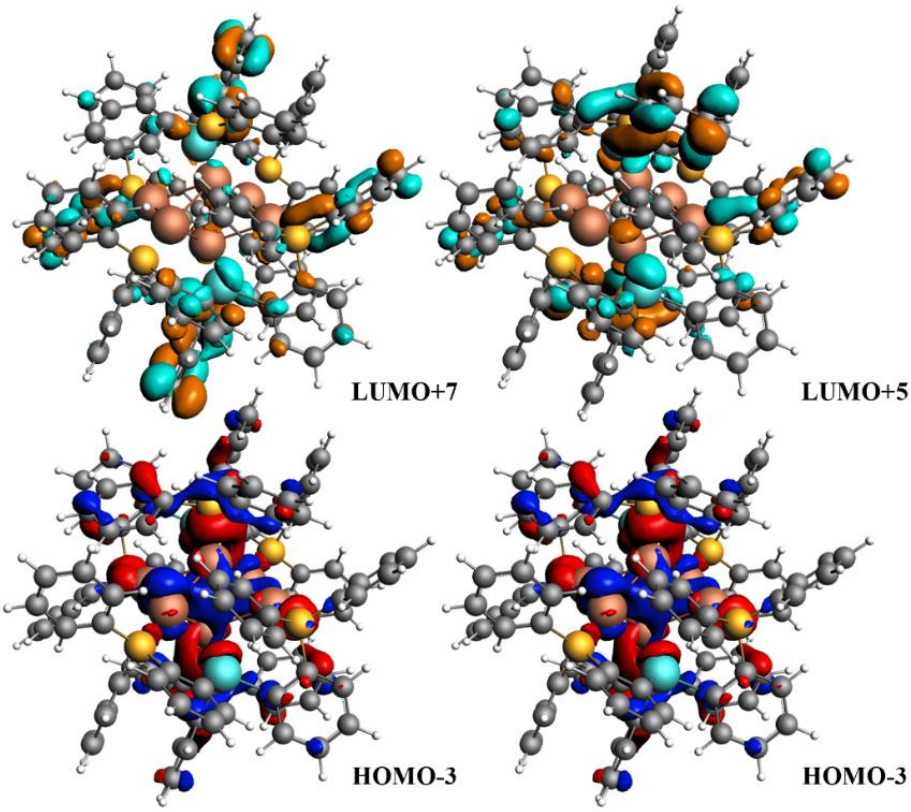

Fig. S10 Molecular orbitals at the BP86-D3/DZP level of theory for the H-3→L+7 and H-3→L+5 transitions in the 3.30 eV peak.

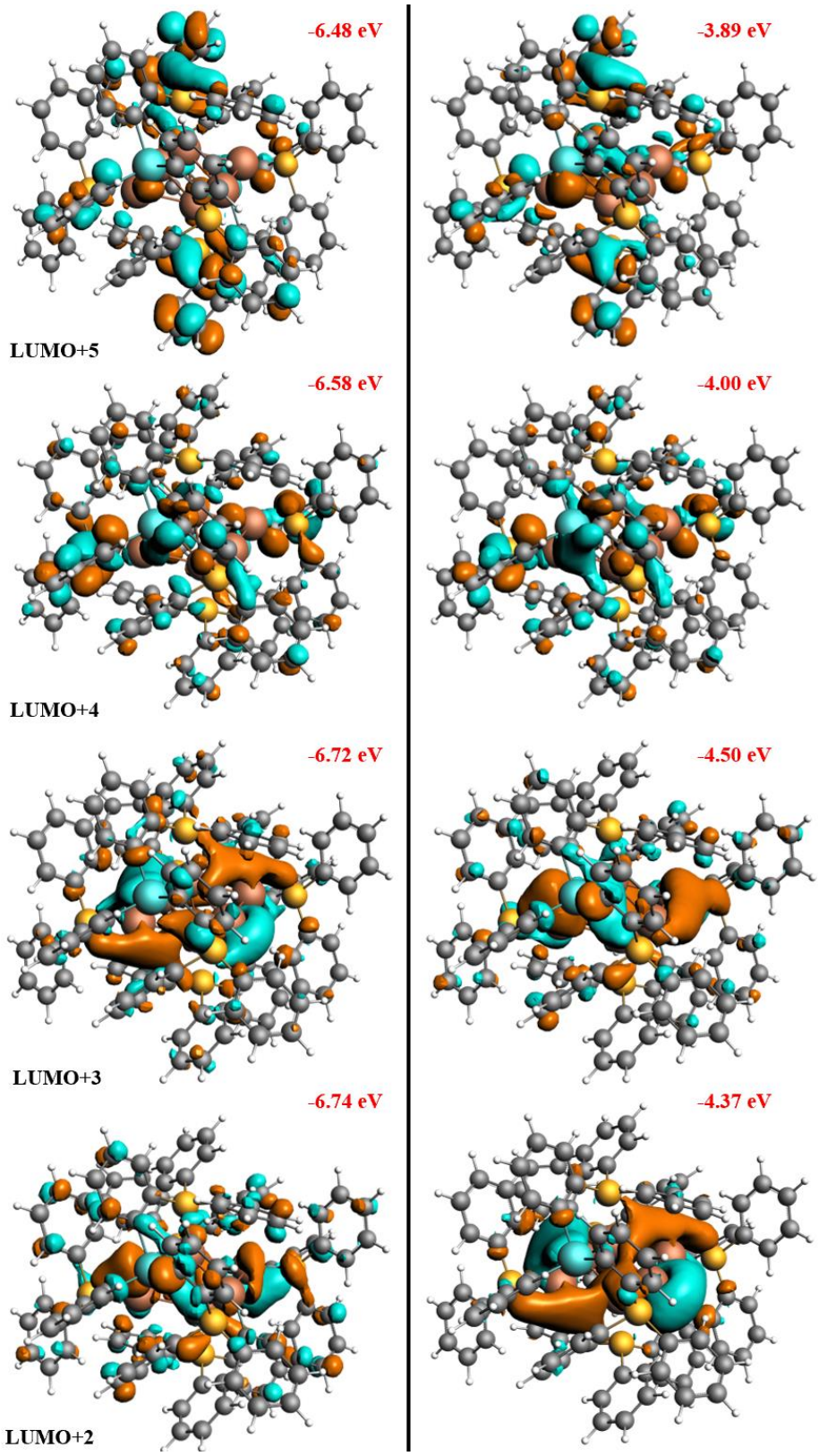

Fig. S11 Molecular orbitals at the BP86-D3/DZP//BP86-D3/DZP (left) and LRCF-D3/DZP//BP86-D3/DZP (right) levels of theory along with the corresponding orbital energy.

.

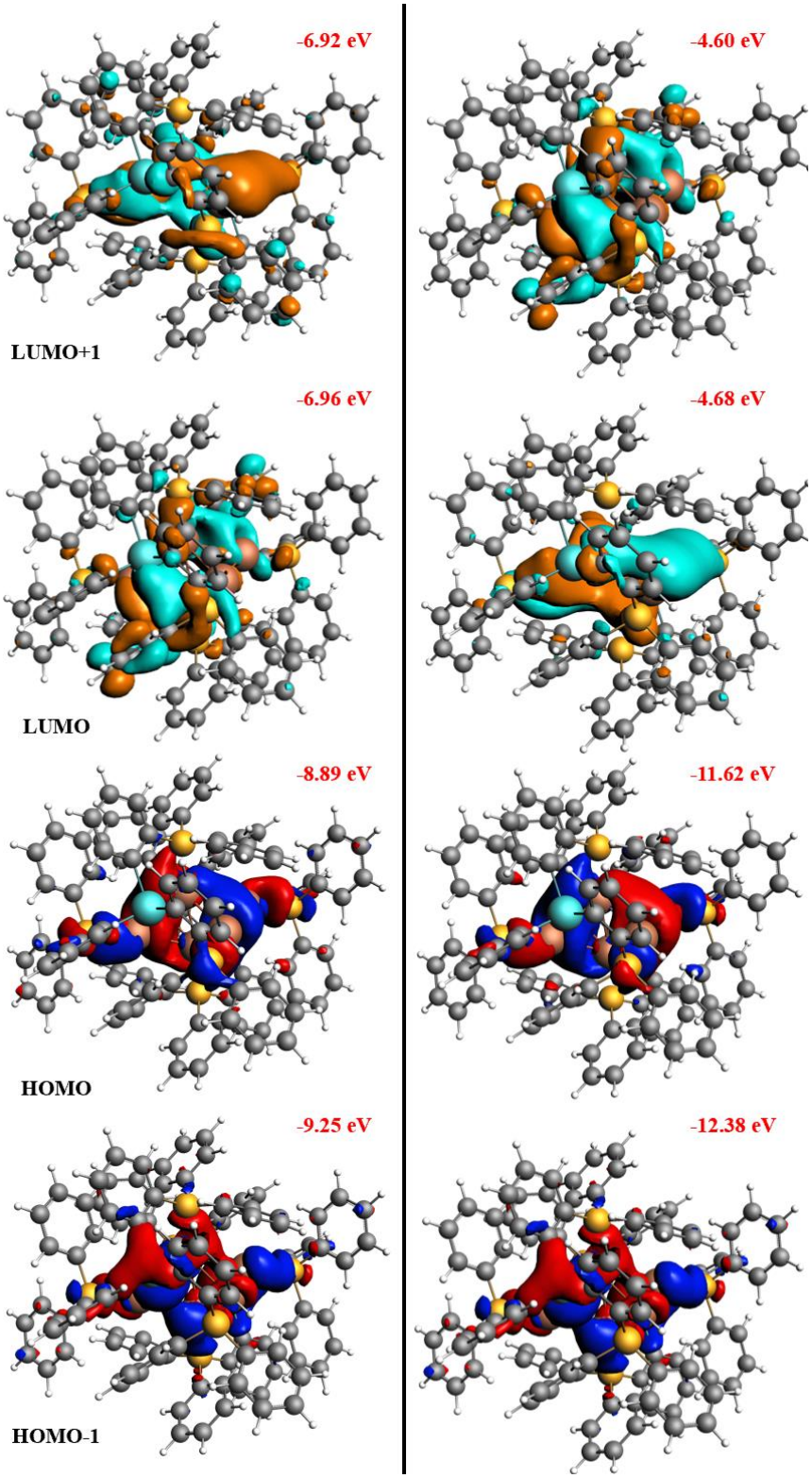

Fig. S12 Molecular orbitals at the BP86-D3/DZP//BP86-D3/DZP (left) and LRCF-D3/DZP//BP86-D3/DZP (right) levels of theory along with the corresponding orbital energy for LUMO+1 – HOMO-1.

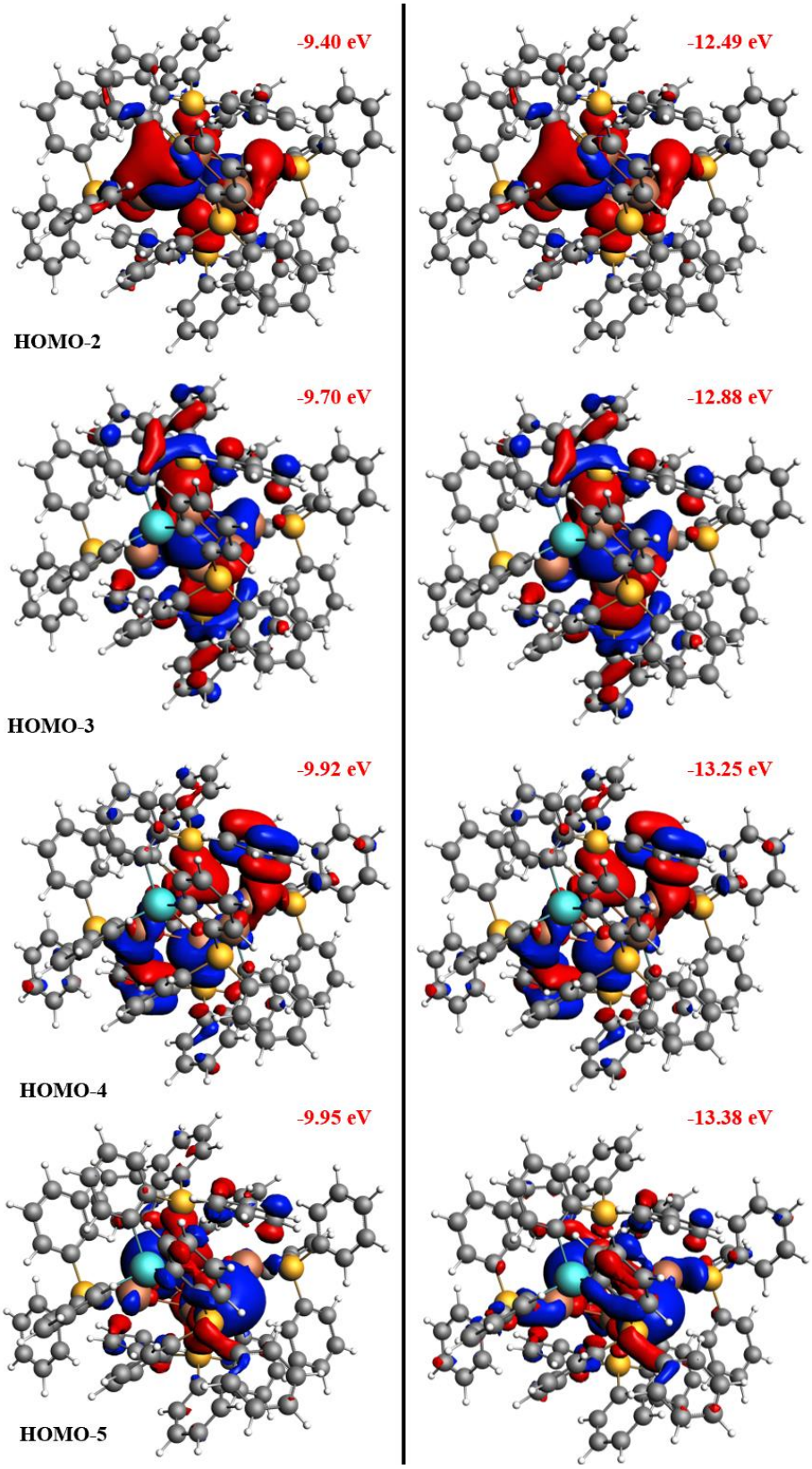

Fig. S13 Molecular orbitals at the BP86-D3/DZP//BP86-D3/DZP (left) and LRCF-D3/DZP//BP86-D3/DZP (right) levels of theory along with the corresponding orbital energy for HOMO-2 – HOMO-5.

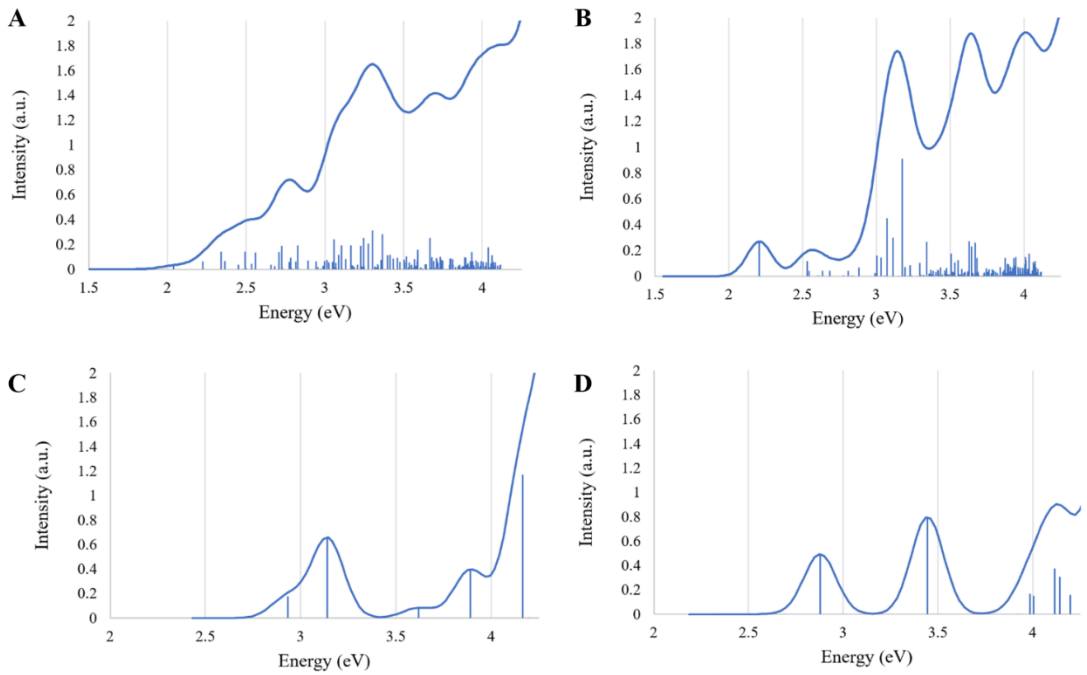

Fig. S14 Absorption spectrum of $[Au_6(SbP_3)_2]^{2+}$ at (A) BP86-D3/DZP//BP86-D3/DZP level of theory and (C) LRCF-D3/DZP//BP86-D3/DZP level of theory. Absorption spectrum of $[Au_6(PPh_3)_6]^{2+}$ at (B) BP86-D3/DZP//BP86-D3/DZP level of theory and (D) LRCF-D3/DZP//BP86-D3/DZP level of theory. (FWHM = 0.20 eV)

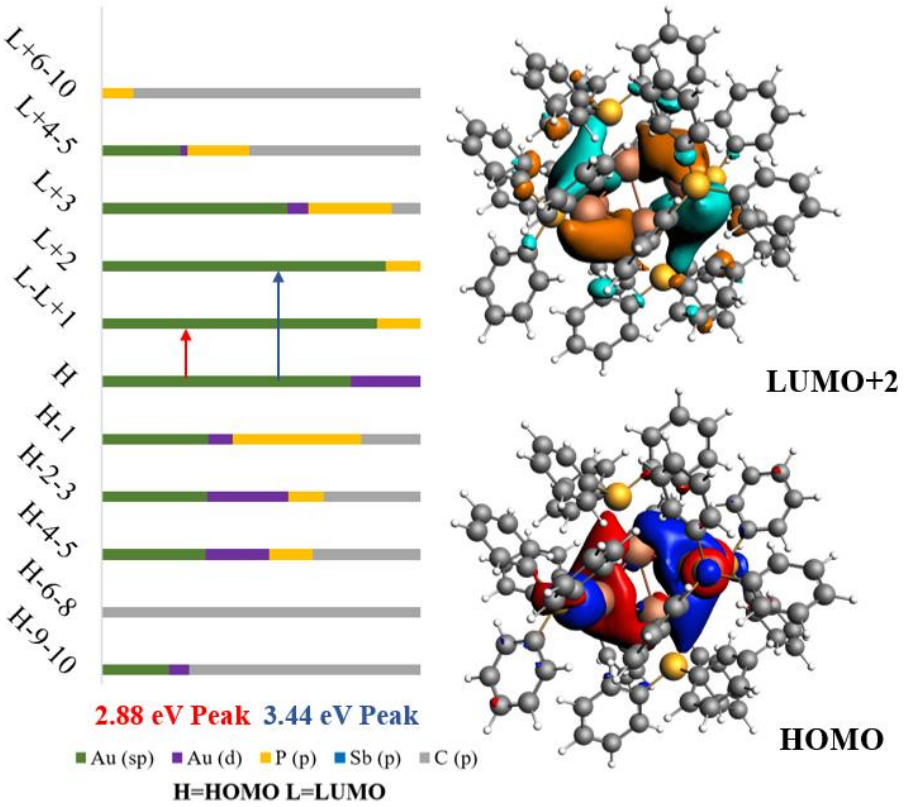

Fig. S15 Molecular orbital details at the LRCF-D3/DZP level of theory at the BP86-D3/DZP S_0 geometry for $[Au_6(PPh_3)_6]^{2+}$. (A) Atomic orbital contributions to molecular orbitals and (B) Molecular orbitals responsible for the 3.44 eV peak.

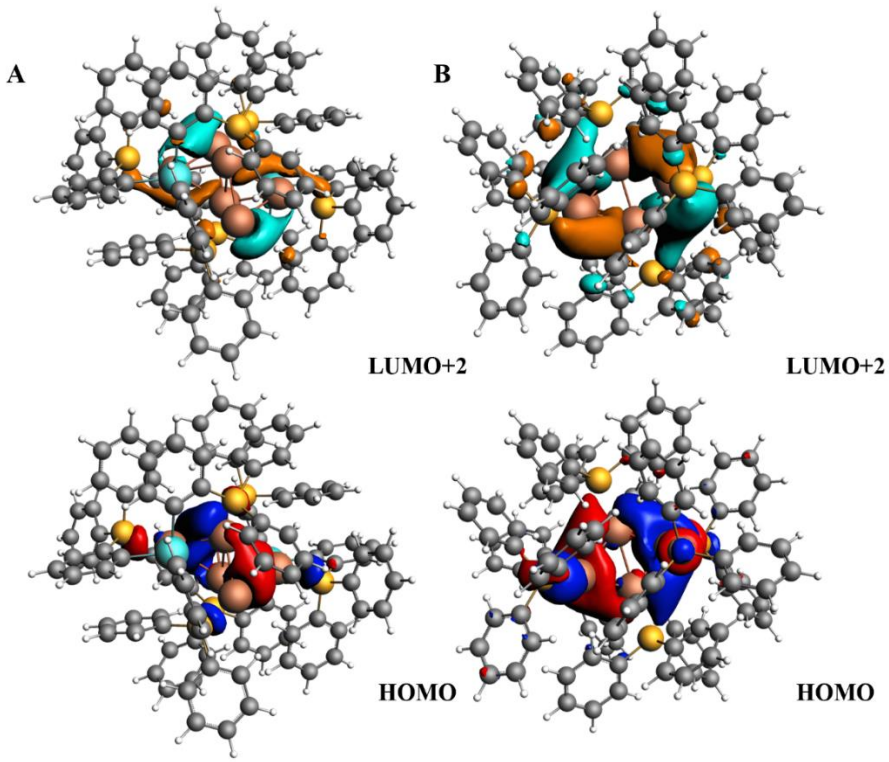

Fig. S16 Molecular orbitals at the LRCF-D3/DZP level of theory on the BP86-D3/DZP S_0 geometry for (A) the H→L+2 transition in the 3.14 eV peak in $[Au_6(SbP_3)_2]^{2+}$ and (B) the H→L+2 transition in the 3.44 eV peak in $[Au_6(PPh_3)_6]^{2+}$.

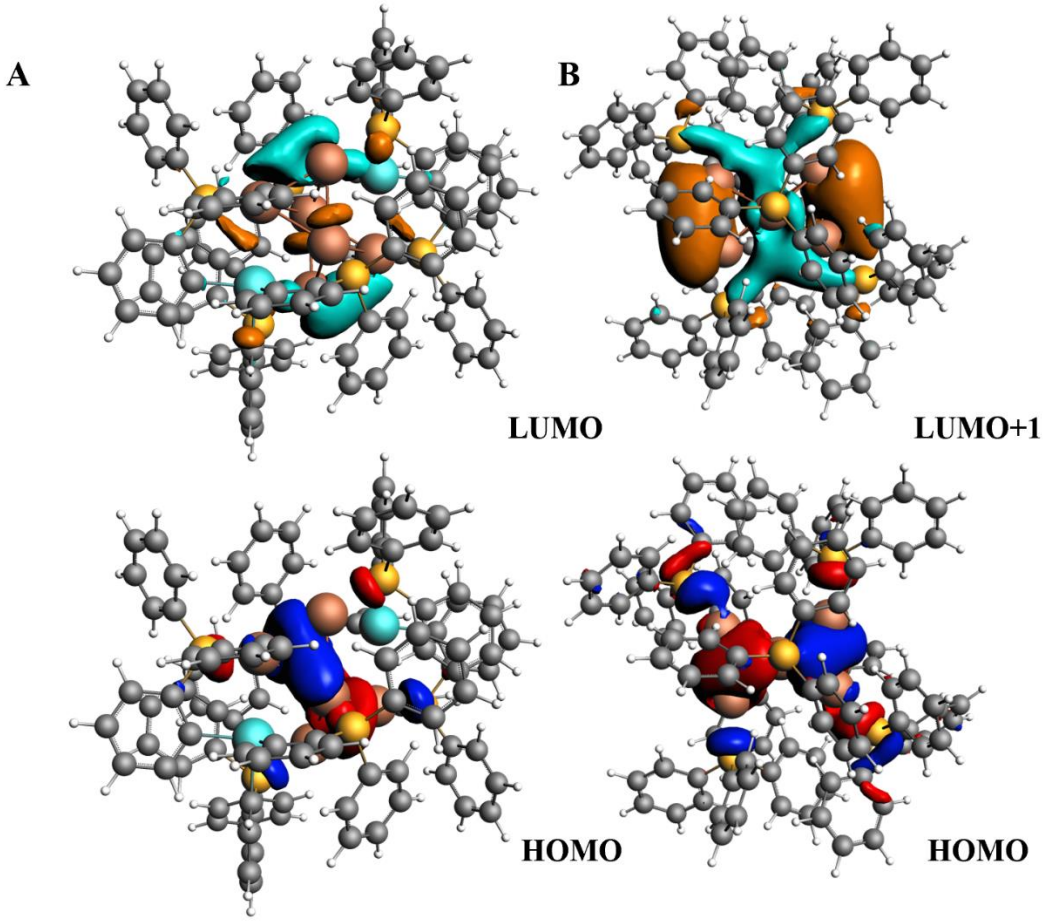

Fig. S17 Molecular orbitals at the LRCF-D3/DZP level of theory on the BP86-D3/DZP S_0 geometry for (A) the H→L transition in the 2.93 eV peak in $[Au_6(SbP_3)_2]^{2+}$ and (B) the H→L+1 transition in the 2.88 eV peak in $[Au_6(PPh_3)_6]^{2+}$.

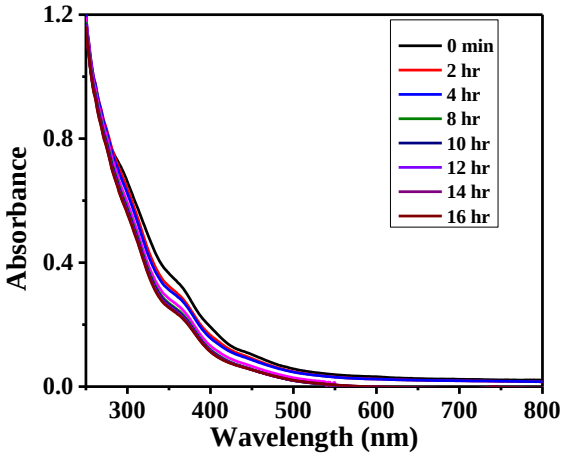

Fig. S18 Time-dependent UV–visible spectral study of thermal stability of a toluene solution of the $[Au_6(SbP_3)_2][PF_6]_2$ cluster at 70 °C.

S1.4 Synthesis of the ligand SbP2.

Trichloroantimony, $SbCl_3$, (1.13 g, 5.33 mmol) and triphenylantimony, $SbPh_3$, (0.94 g, 2.67 mmol) were stirred together solvent-free for 72 h at 25 ºC under argon atmosphere to afford viscous oil of phenylantimony dichloride ($PhSbCl_2$) in quantitative yield. Further, synthetic procedure of the ligand SbP3 was followed to obtain ligand SbP2. 500 mg (1.46 m-moles) of (2-bromophenyl) diphenyl phosphine was dissolved in dry diethyl ether (40 mL) in a 2-necked round-bottomed (RB) flask under argon atmosphere. Solution was cooled to -78°C in acetonitrile-dry ice bath. Then, 1 mL (1.6 M) n-butyllithium is slowly added using a syringe. The reaction mixture is allowed to stir for 30 minutes at -78°C. Then, 198 mg (0.73 m-moles) of phenylantimony dichloride ($PhSbCl_2$) was dissolved in dry diethyl ether (20 mL) under argon atmosphere and was added dropwise using a syringe, while maintaining the temperature at -78 °C. After completion of addition, the reaction mixture was allowed to warm up to room temperature and kept under stirring condition overnight. The product forms as a white precipitate which is then filtered, and washed several times with diethyl ether under argon atmosphere. White solid product was characterized using NMR.

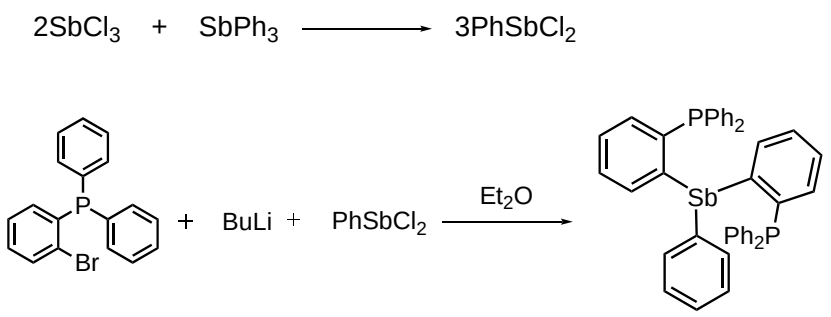

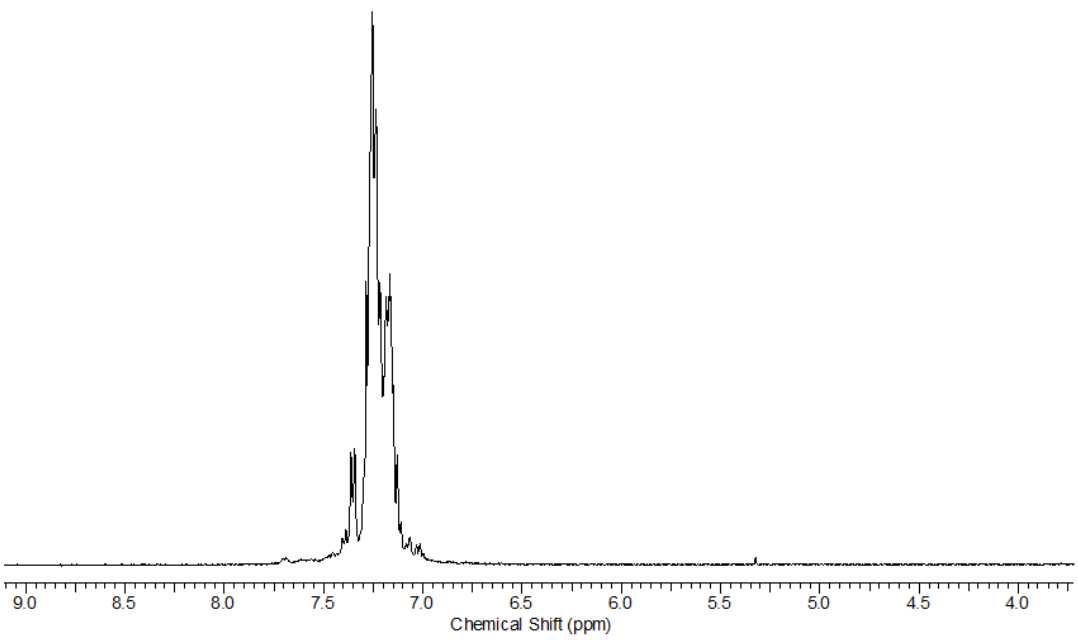

Fig. S19 The ^{1}H-NMR spectra of SbP_2 in $CDCl_3$

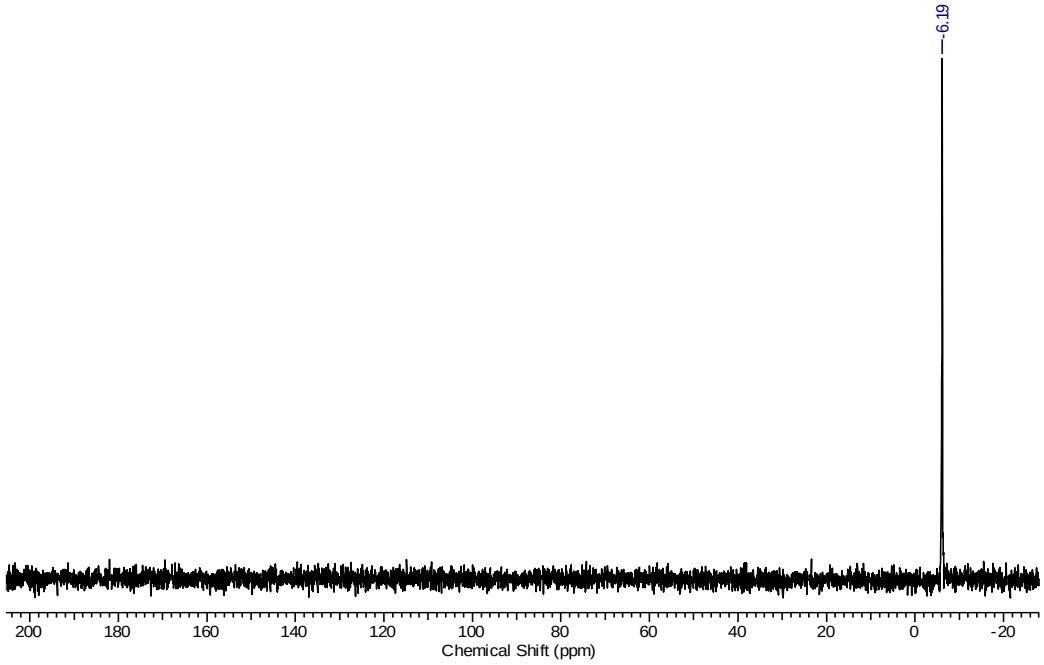

Fig. S20 ^{31}P-NMR spectra of SbP_2

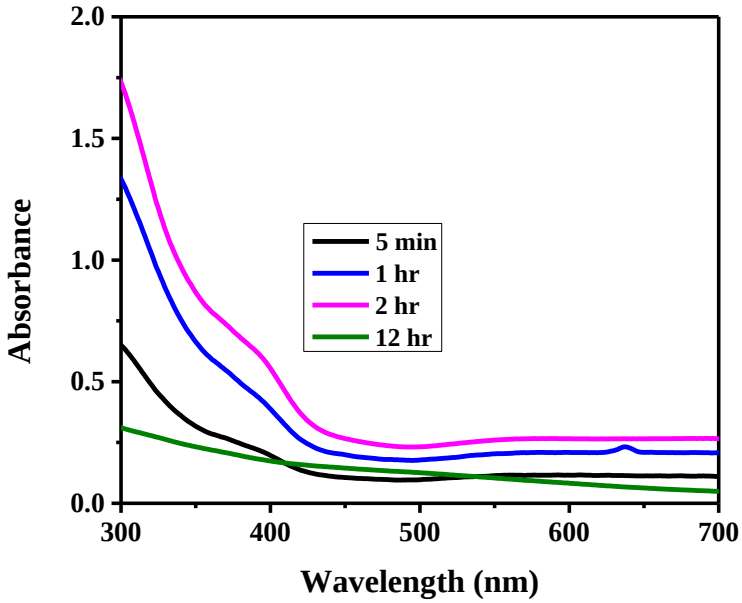

Fig. S21 Time-dependent UV–vis spectra of the cluster formation reaction with SbP_2 ligand.

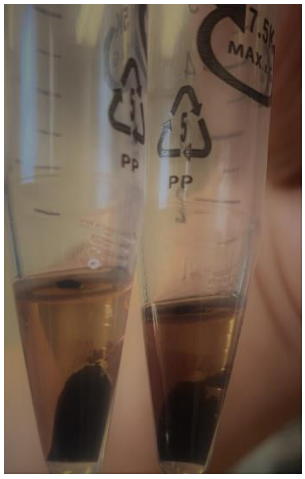

Fig. S22 Picture of the insoluble black precipitate which the unstable Au clusters formed with SbP_2 ligand convert to over time.

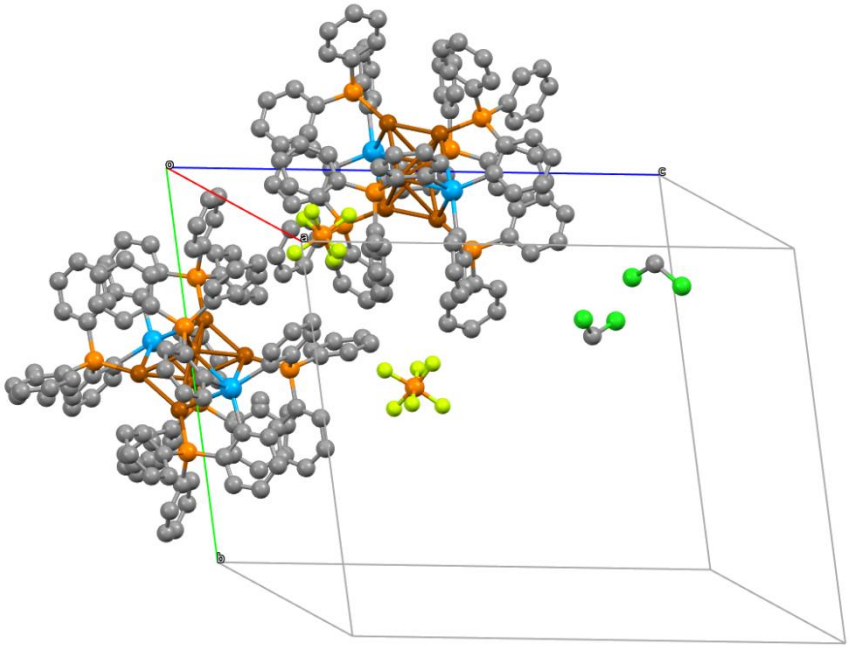

Fig. S23 Crystal packing in the unit cell of the $[Au_6(PPh_3)_2][PF_6]_2$ structure (Colour labels: brown = Au; orange = P; blue = Sb, grey = C; green = Cl; H atoms are not shown for clarity).

References:

[1] J. S. Jones and F. P. Gabbai, "Coordination-and redox-noninnocent behavior of ambiphilic ligands containing antimony", Accounts of Chemical Research **49**, 857-867 (2016).

[2] I.-S. Ke and F. P. Gabbai, "σ-Donor/acceptor-confused ligands: the case of a chlorostibine", Inorganic Chemistry **52**, 7145-7151 (2013).

[3] C. E. Briant, K. P. Hall, D. M. P. Mingos and A. C. Wheeler, *J. Chem. Soc., Dalton Trans.*, 1986, 687-692.